Development of an IPMSM for In-Wheel type Electric Vehicles

Byeong-Hwa Lee, Jeong-Jong Lee, Sung-Il Kim, Soon-O Kwon, and Jung-Pyo Hong
Department of Automotive Engineering, Hanyang University, Seoul 133-791, Korea
E-mail: lbhwa@hanyang.ac.kr, hongjp@hanyang.ac.kr

Abstract — This paper deals with a design approach to an interior permanent magnet synchronous motor (IPMSM) used in in-wheel motor drive systems of electric vehicles. The approach is divided into three parts overall. First, the constant power region of IPMSM and gear ratio are investigated in order to meet the specifications of the in-wheel motor system. Second, the range of inductance and back-EMF to satisfy the given design conditions of the IPMSM is estimated. Finally, the preliminary geometry satisfying the range is decided by PM type, current density, and fill factor and so on, and then the detailed design is carried out by means of finite element analysis in consideration of magnetic saturation.

I. Introduction

Nowadays, a great interest is focused on more efficient and reliable propulsion systems of electric vehicles (EVs) because of an exhaustion of petroleum resources and environmental problem. In general, the propulsion system for EVs consists of batteries, electric motors with drives, and transmission gears to wheels. However, if an in-wheel motor system is applied as the power system of EVs, the transmission composed of many components can be eliminated. Thus, the transmission losses are minimized, and the operation efficiency and reliability is improved [1]. Moreover, more batteries can be installed in the space that would be occupied by the transmission, which help to increase the driving range per charge. On the contrary, due to the elimination of gears, the system needs to produce the total torque directly into the wheel shaft. Consequently, the size of the system tends to grow [2], [3]. Accordingly, for the miniaturization, a planetary gear system is applied in the in-wheel motor system treated in this paper.

In recent years, induction motor drives are preferred for the EV propulsion system owing to their low cost, high reliability, and manufacturing facilitation. However, due to relatively low power density and efficiency, the motor has a drawback in the in-wheel motor system where space and energy savings are critical. Thus, interior permanent magnet synchronous motors (IPMSMs) featuring compactness and high efficiency have become an alternative for the EV propulsion system.

In this paper, a design approach to the IPMSM employed in in-wheel motor system is presented, and it is divided into three parts overall. First, before the shape design of IPMSM, the constant power speed range (CPSR) of the motor and the ratio of a reduction gear satisfying the specifications of in-wheel motor system are determined. Second, the range of inductance and back-EMF to satisfy the required efficiency and output performance of IPMSM is estimated. Finally, the preliminary geometry satisfying the range is decided by PM type, current density, and fill factor and so on, then the detailed design is performed with finite element analysis (FEA) in consideration of magnetic saturation and operating temperature.

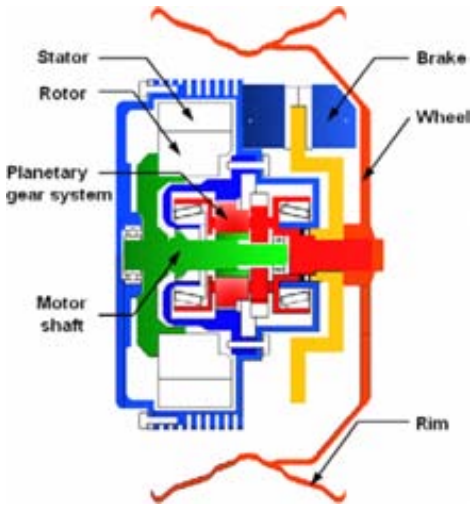

Fig. 1. Assembly configuration of in-wheel motor drive system.

II. Specifications of In-Wheel Motor Drive System

The assembly configuration of in-wheel motor system is shown in Fig. 1. It consists of four parts: motor, reduction gear, brake, and wheel. The specifications of an EV are illustrated in Table I. The road load on the vehicle is composed of three components: aerodynamic drag force F_{ad}, rolling resistance force F_{rr}, and climbing force F_c, which are expressed as follow:

$$F_{ad} = 0.5\rho A C_d v^2 \tag{1}$$

$$F_{rr} = \mu_r mg \tag{2}$$

$$F_c = mg\sin\theta \tag{3}$$

where ρ: the air density; A: the frontal area of the car; C_d: the aerodynamic drag coefficient; v: the relative vehicle velocity to the head wind; μ_r: the rolling friction coefficient; m: the curb mass; θ: the inclination angle of the road.

TABLE I
SPECIFICATIONS OF AN ELECTRIC VEHICLE

Items	Value
Curb mass	1000 kg
Cruising and max. speed	40 / 60 km/h
Acceleration 0-40km/h	Within 5 sec.
Max. climbing slope	30% (16.7°)
Aerodynamic drag coefficient C_d	0.35
Rolling friction coefficient μ_r	0.013
Frontal area A	2.5 m^2
Air density ρ	1.1774 kg/m^3 @ 27°C
Gear efficiency	0.95
Effective radius of tire	0.3262 m (195/55R/16)
Number of rear driving wheels	2

The force required to reach the prescribed acceleration a by overcoming the road load is as follow:

$$F = ma + F_{ad} + F_{rr} + F_c = \frac{G}{r} \cdot T \tag{4}$$

where G: the gear ratio; r: the effective radius of the tire; T: motor torque.

Based on the specifications, the required motor torque and the corresponding speed under various operation conditions of the vehicle are shown in Fig. 2 and Fig. 3 [4]. At this time, the maximum output power of the motor is 25kW.

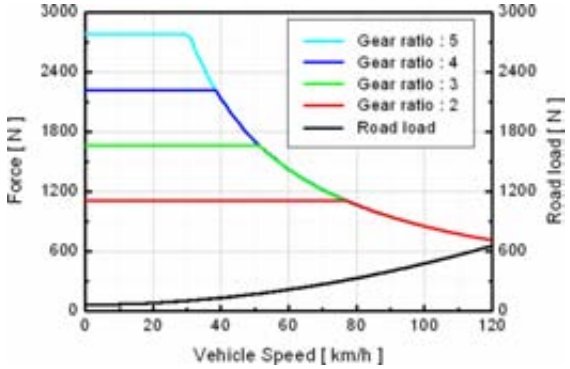

(a) At CPSR 4:1

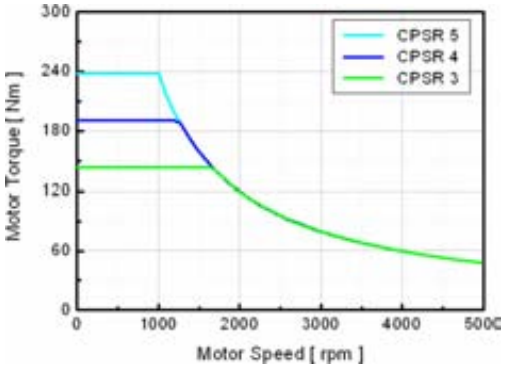

(b) At gear ratio 5:1

Fig. 2. Force and motor torque curve according to gear ratio and CPSR

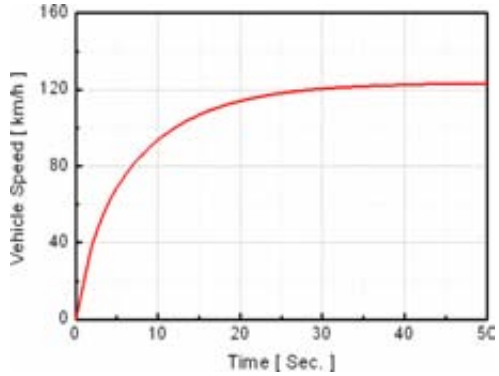

(a) Acceleration capability on 0° slope

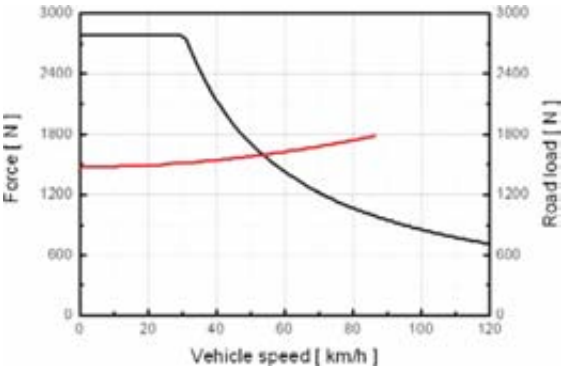

(b) Climbing capability on 16.7° slope

Fig. 3. Acceleration and climbing capability curve of electric vehicle.

III. IN-WHEEL MOTOR DESIGN

A. Range of Back-EMF and Inductance

The parametric design named in this paper is carried out in order to satisfy the given design conditions of IPMSM applied in the in-wheel driving system. That is, it is to estimate the range of inductance and back-EMF treated as the most critical factors in the initial design of IPMSM. The region is obtained by changing the value of inductance and back-EMF in (5), (6) and (7) expressed as the voltage and torque equation of the IPMSM in the steady-state.

$$\begin{bmatrix} v_d \\ v_q \end{bmatrix} = R_a \begin{bmatrix} i_{ad} \\ i_{aq} \end{bmatrix} + \left(1 + \frac{R_a}{R_c}\right) \begin{bmatrix} v_{ad} \\ v_{aq} \end{bmatrix} \tag{5}$$

$$\begin{bmatrix} v_{ad} \\ v_{aq} \end{bmatrix} = \begin{bmatrix} 0 & -\omega L_q \\ \omega L_d & 0 \end{bmatrix} \begin{bmatrix} i_{ad} \\ i_{aq} \end{bmatrix} + \begin{bmatrix} 0 \\ \omega \psi_a \end{bmatrix} \tag{6}$$

$$T = P_n [\psi_a i_{aq} + (L_d - L_q) i_{ad} i_{aq}] \tag{7}$$

where i_d, i_q: d- and q-axis components of armature current; i_{cd}, i_{cq}: d- and q-axis components of iron loss current; v_d, v_q: d- and q-axis components of terminal voltage; ψ_a: $\sqrt{3/2}\,\psi_f$; ψ_f: maximum flux linkage of permanent magnet; R_a: armature winding resistance; R_c: iron loss resistance; L_d, L_q: inductance along d- and q-axis; P_n: number of pole pairs.

TABLE II
THE REQUIREMENTS FOR IPMSM DESIGN

Items	Value
Stator outer diameter	Less than 280 mm
Stack length	Less than 67 mm
Br (@ 75°C)	1.13 T
Efficiency @ 1500rpm	More than 90 %
DC link voltage	300 V
Maximum line-to-line voltage	197 V
Maximum current	110 A_{rms}
Max. and rated output power	25 / 10 kW
Base and Max. speed	1250 / 5000 rpm
Current density @ Max. and rated output power	Less than 7 / 17 A/mm^2

TABLE III
THE RANGE OF DESIGN FACTORS

Factors	Range
d-axis inductance (L_d)	0.56 ~ 0.64 mH
Phase back-EMF @ 1250rpm	77.5 ~ 83.5 V_{rms}
Saliency ratio	1.5

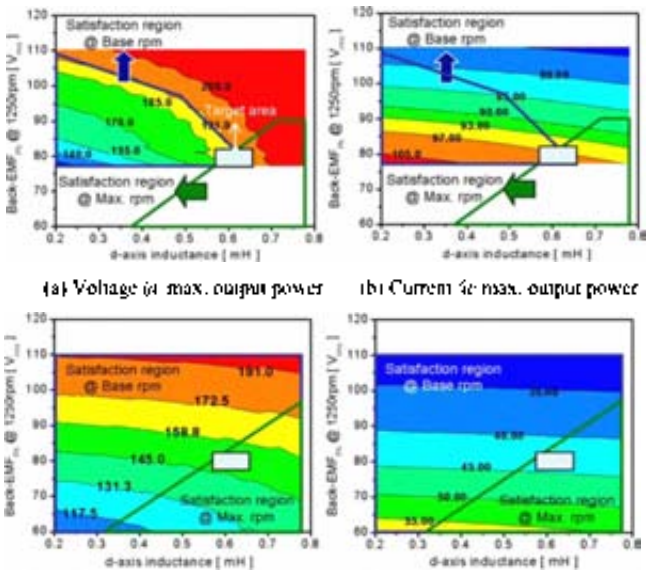

(a) Voltage @ max. output power (b) Current @ max. output power

(c) Voltage @ rated output power (d) Current @ rated output power

Fig. 4. Design region of IPMSM according to back-EMF and inductance.

At that time, some parameters are greatly influenced by past experimental data or designer's experience, and there are assumptions. First of all, the iron loss is neglected. Second, the winding resistance is assumed as 17mΩ at the operating temperature. Third, the ratio between L_d and L_q is 1.5. Finally, mechanical loss is 0.1% of maximum output power at 1000 rpm, and the loss is proportional to the square of speed. The requirements of IPMSM are shown in Table II, and Table III and Fig. 4 display the results obtained by the parametric design.

TABLE IV
THE RESULTS OF INITIAL DESIGN

Items	Value
TRV	91.3 kN-m^3
Stator outer diameter	280 mm
Rotor outer diameter	204 mm
Stack length	67 mm
Number of series turns	79
Calculated winding resistance	18.5 mΩ @ 75°C
Air-gap	0.8 mm
Fill factor	43.1 %
Phase back-EMF @ 1250rpm	77.6 V_{rms}

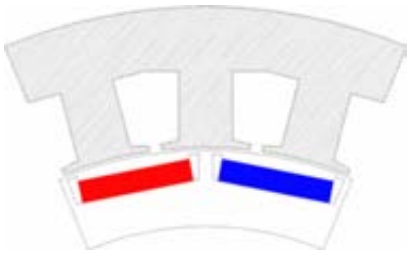

Fig. 5. Initial designed configuration of in-wheel motor

B. Preliminary Geometry

In this section, the procedure for preliminary geometry design of IPMSM is illustrated. Above all, in the process, torque per rotor volume (TRV) according to PM type is estimated within the dimension displayed in Table II [5]. Second, the number of series turns, air-gap length, and PM shape such as pole arc and thickness are determined with an analytical method used for the design of PM synchronous motor [6]. Third, the coil diameter considering current density is selected. At this time, the current is obtained by the parametric design. Finally, the shape of stator is roughly decided by the number of series turns and fill factor, and if the value of back-EMF calculated by finite element analysis (FEA) is included within the range shown in Table III, the initial design is completed. In the end, the final results of initial design are given in Table IV and Fig. 5.

IV. FINITE ELEMENT ANALYSIS

A. Calculation of Inductance

In order to calculate the accurate characteristics of IPMSM designed in Section III, L_d and L_q must be computed according to the variation of armature current and current angle (β). In this paper, they are obtained through FEA, cubic spline interpolation and (8), and their one part is shown in Fig. 6. In (8), ψ_m and ψ_a are fundamental components calculated from fourier analysis.

$$L_d = \frac{\psi_m \cos\alpha - \psi_a}{i_d}, \qquad L_q = \frac{\psi_m \sin\alpha}{i_q} \tag{8}$$

where ψ_a: total flux linkage considering the armature reaction effects; α: phase difference between ψ_a and ψ_m.

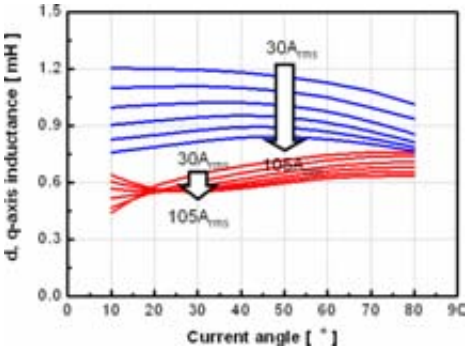

Fig. 6. L_d and L_q of initial model according to current and β.

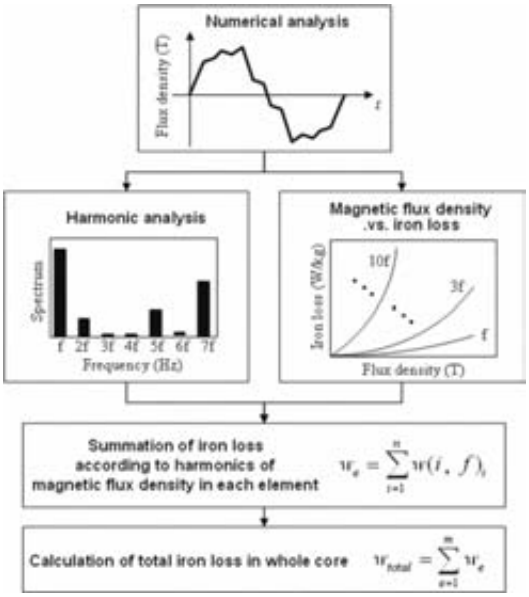

Fig. 7. Iron loss calculation process

B. *Equivalent Iron Loss Resistance*

Fig. 7 shows the process of iron loss calculation using iron loss data of magnetic material. The detailed explanation of the flowchart has been given in [7]. After estimating total iron loss, w_{core}, the iron loss resistance R_c can be computed by (9).

$$R_c = 6,707 \times rpm^{0.499} \tag{9}$$

C. *Characteristic Analysis*

In order to verify the requirements of IPMSM given in Table II, the characteristic analysis are carried out with parameters estimated through the way mentioned above, (5), (6), and (7). At this time, the following limitations on armature current and terminal voltage are considered:

$$I_a = \sqrt{i_d^2 + i_q^2} \le I_{am} \tag{10}$$

$$V_a = \sqrt{v_d^2 + v_q^2} \le V_{am} \tag{11}$$

where I_{am}, V_{am}: peak values of current and voltage.

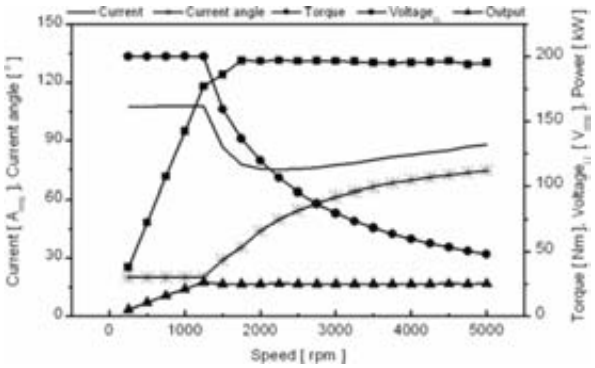

(a) At maximum output power

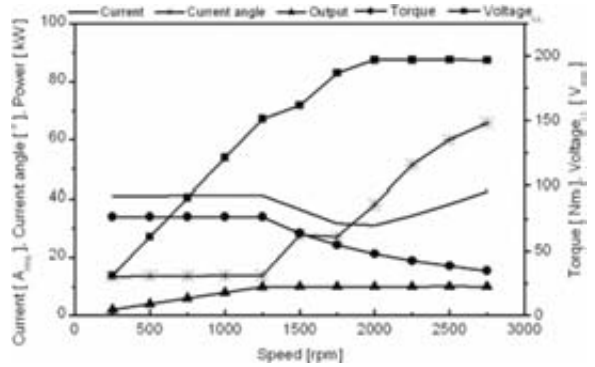

(b) At rated output power

Fig. 8 Characteristic analysis curves of IPMSM

Fig. 8 shows the characteristic analysis results of the IPMSM indicated in Fig. 5. The results are shown in good agreement with those displayed in Fig. 4.

V. Conclusion

In this paper, a design approach to IPMSM for an in-wheel motor driving system was presented. Even if some parameters are assumed in the parametric design stage, the approach is effective for the design of IPMSM.

References

[1] Y. P. Yang and D. S. Chuang, "Optimal design and control of a wheel motor for electric passenger cars," *IEEE Trans. on Magn.*, Vol. 43, No. 1, pp. 51-61, Jan. 2007.

[2] S. Wu, L. Song, and S. Cui, "Study on improving the performance of permanent magnet wheel motor for the electric vehicle application," *IEEE Trans. on Magn.*, Vol. 43, No. 1, pp. 438-442, Jan. 2007.

[3] K. M. Rahman, N. R. Patel, T. G. Ward, J. M. Nagashima, F. Caricchi, and F. Crescimbini, "Application of direct-drive wheel motor for fuel cell electric and hybrid electric vehicle propulsion system," *IEEE Trans. on Industry Applicat.*, Vol. 42, No. 5, pp. 1185-1192, Sep./Oct. 2006.

[4] M. Ehsani, Y. Gao, S. E. Gay, and A. Emadi, *Modern electric, hybrid electric, and fuel cell vehicles*, CRC Press, 2005.

[5] J. R. Hendershot Jr. and T. J. Miller, *Design of brushless permanent-magnet motors*, Oxford University Press, 1994.

[6] A. M. EL-Refaie and T. M. Jahns, "Optimal flux weakening in surface PM machines using fractional-slot concentrated windings," *IEEE Trans. Ind. Applicat.*, vol. 41, no. 3, pp. 790-800, May/June 2005.

[7] J. J. Lee, Y. K. Kim, H. Nam, K. H. Ha, J. P. Hong, and D. H. Hwang, "Loss distribution of three phase induction motor fed by pulsewidth modulated inverter," *IEEE Trans. Magn.*, vol. 40, no. 2, pp. 762-765, March 2004.